Nuclear Instruments and Methods in Physics Research A 737 (2014) 33–41

Contents lists available at ScienceDirect

Nuclear Instruments and Methods in Physics Research A

journal homepage: www.elsevier.com/locate/nima

# Time correlation of cosmic-ray-induced neutrons and gamma rays at sea level

G. Miloshevsky *, A. Hassanein

*Center for Materials Under Extreme Environment, School of Nuclear Engineering, Purdue University, 400 Central Drive, West Lafayette, IN 47907-2017, USA*

ARTICLE INFO

*Article history:*
Received 4 October 2013
Received in revised form
5 November 2013
Accepted 8 November 2013
Available online 18 November 2013

*Keywords:*
Cosmic rays
Multiplicity
Coincidence
Correlation
Poisson distribution
Feynman-Y statistic

ABSTRACT

The neutrons and gamma rays produced by cosmic ray interactions in spallation and evaporation processes of air nuclei are time-correlated. The occurrence of their counts in a fixed time interval is not a random (Poisson) distribution, but rather time-correlated bursts of counts. A computational model is developed to explore time correlations of cosmic-ray-induced background of neutrons and gammas at sea level. Their lifetimes in air showers, multiplicity distributions, coincidence count statistic, and excess variance are analyzed. The effects of latitude and area size on multiplicity and coincidence distributions are also studied. The coincidence count distributions and Feynman-Y statistic are used to reveal the duration of spallation processes and properties of multiplying media. It is found that the coincidence count distribution in fixed time intervals deviates from a Poisson distribution. The Feynman-Y is about an order of magnitude greater for gammas than that for neutrons. For both neutrons and gammas, the duration of time-correlated multiplying processes in air showers is ~250 μs.



## 1. Introduction

Primary cosmic rays incident upon the Earth's atmosphere mainly consist of protons (about 87 percent) [1]. After impacting the upper atmosphere, high-energy protons interact with air nuclei generating a cascade air shower. At the Earth's surface, the background radiation consists of neutrons and protons (nucleonic component), electrons and gammas (soft component), and muons (hard component) [2–6]. A vast amount of experimental and theoretical data is available on cosmic rays in the Earth's atmosphere, at sea level, and underground [3]. Many of the studies have been focused on nuclear interactions and spatial structure of air showers [7,8], their propagation [9], composition [10], energy and angular spectra of particles [11,12]. Several attempts have been made to study the longitudinal structure of the shower core by investigating the arrival-time distribution of shower particles. In pioneering work of Bassi et al. [13], the instantaneous spatial distributions of particles in extensive air showers at sea level have been studied by measuring their times of arrival. It was found that the electron–photon component is confined in a thin disk of thickness 1–2 m, slightly in advance of a thicker muon disk. Further experiments [14–17] have revealed more details in the structure of air-shower electrons both near and far from the core axis. The arrival time of muons have been studied using high-speed recordings in order to clarify their longitudinal development through the atmosphere [18–20]. Monte Carlo calculations on the arrival time distribution of particles in air showers have been also carried out [21,22]. These studies of individual extensive air showers have utilized the time distributions of air-shower particles in order to derive information concerning their longitudinal evolution, arrival direction, and shower composition.

Rather less attention has been paid to the analysis of arrival times of particles using statistical techniques for analyzing time correlations, mean values, dispersion and multivariate distributions, although some work has been done in this direction for both the individual air showers and the background radiation of particles at sea level. Theoretical methods of nonlinear analysis have been applied to study the bursts of the count rate of extensive air showers and the correlation of their time series that represent shower arrival times [23]. Large-scale correlations and coincidences in arrival time of extensive air showers have been investigated using ten independent stations scattered over a very large area [24]. The time correlation of cosmic-ray-induced background of neutrons and gammas at sea level has been also investigated to some degree [25–27]. However, the statistical aspects of time correlations such as multiplicities, coincidence count statistic, and excess variance of neutrons and gammas were not analyzed. The importance of statistical methods in the analysis of the temporal and spatial features in cosmic ray data was highlighted by Orford [28]. It is a well established fact that the majority of neutrons is produced in spallation and evaporation processes of air nuclei [2,3]. Since each shower is triggered by a

* Corresponding author. Tel.: +1 765 494 8618; fax: +1 765 496 2233.
*E-mail address:* gennady@purdue.edu (G. Miloshevsky).

0168-9002/$ - see front matter © 2013 Elsevier B.V. All rights reserved.
http://dx.doi.org/10.1016/j.nima.2013.11.036

single proton, all the secondary neutrons and gammas are, to some extent, time-correlated. Thus, neutrons and gammas produced by cosmic ray interactions with air nuclei are not Poisson distributed (not independent random events), but can be characterized by bursts of time-correlated counts [27].

The spread in arrival time and coincidence correlations of neutrons and gammas in the air shower are of fundamental and practical significance. From the point of view of fundamental science, these distributions can reveal the duration of spallation processes and excess variance compared to a random Poisson distribution. The properties of the multiplying medium can be deduced through a statistical distribution of counts. Practical importance is related to the detection of Special Nuclear Materials (SNM) [29–31]. These materials emit multiple neutrons and gammas simultaneously, very unique time-correlated signatures, via spontaneous or induced fission. The fact that SNM emits multiple neutrons simultaneously (time-correlated) is used in modern neutron detectors to detect fission events. These two features, multiplicity and time-correlation, are the way of distinguishing the different types of neutrons. However, the neutron detectors are unable to discriminate time-correlated neutrons induced by cosmic events from those emitted by a fission source. The neutron and gamma background produced by cosmic rays can be comparable or even more intense than that from fission of highly enriched uranium (HEU), making the detection of HEU extremely difficult [32,33]. If the SNM multiplicity and coincidence distribution can be uncoupled from cosmic-ray interferences, then the identity of a fission source can be determined. However, the arrival time, coincidence correlations, large-scale structure, angular, energy and area distributions of neutrons and gammas from atmospheric cascade showers at sea level are not understood. There is a need in analyzing the arrival time of cosmic-ray-induced neutrons and gammas and understanding their multiplicity, coincidence count and excess variance distributions.

The goal of this study is to gain a better understanding of time-correlation of cosmic-ray-induced background of neutrons and gammas at sea level. We have developed and implemented the statistical methods in order to analyze the stream of arrival times of neutrons and gammas, and investigated their lifetimes and multiplicity distributions in air showers, coincidence count statistic, and excess variance. The effects of latitude and the size of area on these distributions are studied. The paper is organized as follows: in Section 2 we describe the computational models; in Section 3 the results are presented; Section 4 contains discussion; and conclusions are provided in Section 5.

## 2. Computational models

Our specific goal is to analyze the arrival times of neutrons and gammas from multiple air showers (i.e. radiation background) within a specified area at sea level. Their times of arrival are sampled using the cosmic-ray shower library (CRY) [34] that is described below in this section. In order to register arrival times, distinct time axes are introduced for neutrons and gammas. Time points corresponding to arrival times of neutrons or gammas are stored in arrays. The arrival-time statistic is accumulated over several days accounting for billions of air showers. The huge stream of arrival times then serves as an input for the statistical models that are developed and implemented in our MONSOL code. The code calculates lifetime, multiplicity, coincidence count distributions and Feynman-Y statistic.

### 2.1. Calculation of neutron and gamma lifetimes in air showers

The lifetime distribution of neutrons and gammas in air showers is calculated as follows. For each individual air shower, a clock starts at $t=0$ with a proton impacting the top of the atmosphere. The clock continues to run, and proton-induced cascades of secondary particles are developed. The lifetime of particles in air shower is defined as the time between the particle being born in the atmosphere at some point and the time it is arrived at sea level. Some secondary particles are absorbed, before they can reach sea level. New particles generated in spallation reactions close to sea level may have very short lifetimes. Particles with long lifetimes are produced in evaporation decays of air nuclei. Therefore, lifetimes of neutrons and gammas can vary from microseconds to seconds. The clock stops when all neutrons and gammas are counted from a particular air shower at sea level within a specified area. The distribution of lifetimes is then calculated as an average of neutron and gamma lifetimes in individual air showers.

### 2.2. Calculation of neutron and gamma multiplicity

Multiplicity means the frequency of the occurrence of 0, 1, 2, etc. neutrons or gammas at sea level within a specified area for each of individual air showers. To calculate multiplicity distributions, the number of neutrons and gammas at sea level is counted for succeeding air showers. The multiplicity distribution is then constructed as an average of multiplicities of individual air showers.

### 2.3. Calculation of coincidence counting and Feynman variance-to-mean statistic

In order to calculate the coincidence count distribution and the excess variance-to-mean ratio (Feynman-Y statistic), each time axis is divided into time bins of a predetermined time period, the length of which can be different for each of particles [28]. The schematic is illustrated in Fig. 1 with particular time bin widths of $\tau=100$ μs and $\tau=10$ μs for neutrons and gammas, respectively. The arrival time data are then analyzed in fixed time bins with different width $\tau$ (400 time distributions were analyzed with widths of 5 μs, 10 μs,… 2000 μs) imposed on the stream of neutron and gamma counts. Let us focus on the stream of neutron counts. After the simulation is finished, there are $n_0$ time bins with 0 neutron counts, $n_1$ time bins with 1 neutron counts, etc. The time bins are then arranged in increasing order of the number of counts $k=0, 1, 2,\ldots$ For each of 400 time widths, the coincidence count distributions $\Omega(k,\tau)$ as a function of $k$ is built by normalizing $n_k$ to the total number of time bins $K$. Finally, there are 400 distributions $\Omega(k,\tau)$ with fixed bin widths of $\tau=5$ μs, 10 μs, 15 μs,… 2000 μs. The derived coincidence count distributions are further processed for estimates of mean and variance. The mean $\mu$ is calculated as the average number of counts $\mu=<k>$ in time bins with width $\tau$. The variance is then determined as the mean of the

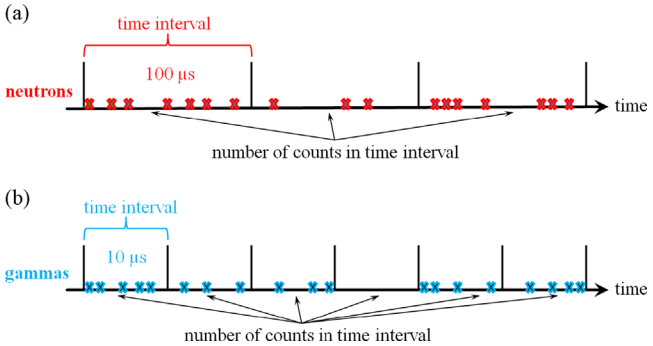


**Fig. 1.** Representative sketch illustrating the number of (a) neutron and (b) gamma counts within fixed time intervals with particular widths 100 μs and 10 μs, respectively. Particle counts are marked by cross symbols (x).

count squares minus the square of the mean, i.e., $\sigma^2 = < k^2 > - < k >^2$. The variance-to-mean ratio is used to analyze the streams of neutrons and gammas for time correlations. This approach is called the Feynman-Y statistic [35]. The parameter $Y$ is defined as $Y = \sigma^2/\mu - 1$. If all counts of particles in time bins are statistically independent, they will have a Poisson distribution with the mean equal to the variance resulting in $Y = 0$. In a cascade air shower, however, time-correlated neutrons and gammas are produced due to spallation-type nuclear processes. Bursts of counts will occur in time bins due to multiple events caused by cosmic rays. Time correlations will lead to a variance higher than Poisson's variance resulting in $Y > 0$. This excess variance in coincidence count distributions of time-correlated particles compared to the variance of a Poisson distribution with the same mean is the basis of the Feynman variance-to-mean method [35].

### 2.4. Cosmic-ray shower library

We use the CRY library [34] developed at Lawrence Livermore National Laboratory (LLNL) in order to generate the stream of arrival times of neutrons and gammas at sea level. The CRY library contains precomputed data tables derived from the full MCNPX simulation of primary protons in the energy range of 1 GeV–100 TeV incident on the top of the atmosphere. The technical details of MCNPX simulations are not published. Therefore, we briefly outline the setup of the simulation system as described in Ref. [34]. In that MCNPX simulation, the energy $E$ of cosmic protons at the top of the atmosphere was sampled from a simple analytic expression $J(E) = A(E+B)^{\alpha}E^{\beta}$ protons/(m$^2$ sr s GeV) with fitted parameters $A$, $B$, $\alpha$, and $\beta$ given in Ref. [36]. This parameterization is the best fit to the observed energy spectrum of primary protons. The parameters $B$, $\alpha$ and $\beta$, are used to modulate the minimum and maximum solar activity. For a specific date of the year, the proton flux was calculated as a weighted sum of the solar-min and solar-max flux [34]. The direction of incident protons was sampled using an isotropic angular distribution. The 1976 US Atmosphere Model was used to construct the Earth's atmosphere as a series of 42 air layers with a constant density. The air density is changed by 10% between adjacent layers. The composition of air is 78% $N_2$, 21% $O_2$, and 1% Ar by volume. The top of the atmosphere was located at ~31 km.

The computer time consuming MCNPX runs performed at LLNL have taken more than 10,000 cpu h [34]. Therefore, precomputed data tables were created as the CRY library. The CRY software library is a very fast tool to generate time-correlated distributions of neutrons, photons, muons, electrons, and pions at altitudes of 0 m, 2100 m, and 11300 m. The particle production with the proper flux can be calculated within a specified area (9 m$^2$, 100 m$^2$, 900 m$^2$, and $10^4$ m$^2$). The effects of latitude (geomagnetic cutoff) and solar cycle can be included. The energy, time of arrival, 3D coordinates, direction cosines, and multiplicity of these particles are sampled for each individual shower. These distributions are validated against available cosmic-ray measurements [34]. The CRY-generated energy spectra of neutrons and gammas were found in a good agreement with data measured at sea level. The neutron background simulated with the CRY library has been recently compared to the measured data demonstrating a very good agreement [37], thus confirming the validity of the CRY data. The CRY library was also used to model the hadronic interactions of cosmic rays with different materials [38,39]. An interface C++ routine for calling the CRY library is implemented in our MONSOL code to generate the stream of arrival times of neutrons and gammas at sea level within a specified area. The post-processing of arrival times is then performed as described above to calculate lifetime and multiplicity distributions, coincidence count distributions, and Feynman-Y statistic.

### 2.5. Simulation set-up

Our simulations are carried out for various latitudes and area sizes of 9 m$^2$, 100 m$^2$, 900 m$^2$, and $10^4$ m$^2$. The solar activity is set to solar minimum corresponding to the maximum flux of cosmic rays. The solar modulation of primary cosmic rays in the heliosphere influences only the low-energy portion of the spectrum [34]. The rate of proton events (number of protons per second) is calculated by integrating the differential spectrum of primary protons with corrections for latitude and solar cycle effects [34]. At latitude of 40°N and minimum solar activity, for instance, the average rate of incident protons with the energy from 1 GeV to 100 TeV is found to be ~18,510 protons/s within the area of 100 m$^2$. The total number of sampled proton primaries is ~$10^{10}$ protons corresponding to the observation time of ~6.25 days. The fraction of time between succeeding protons is ~54 μs. Since this time fraction is small, distinct air showers can overlap in time. Due to a large spread in particle lifetimes, this means that neutrons and gammas from later showers can arrive at sea level before preceding showers are exhausted.

## 3. Results

The stream of arrival times of cosmic-ray-induced neutrons and gammas at sea level is postprocessed in MONSOL to calculate lifetime, multiplicity, and coincidence count distributions as well as Feynman-Y statistic. It is found that the energy of secondary neutrons at sea level is ranged from a few meV up to ~200 GeV. The energy of gammas is found in the range from ~1 MeV up to ~40 GeV. There are only a few neutrons and gammas with energies in the GeV range. We find that at sea level the flux of cosmic-ray-induced gammas and neutrons increases with the increase of latitude. The gamma flux is ~141 gammas/(m$^2$ s) at 0°N, ~152 gammas/(m$^2$ s) at 20°N, ~175 gammas/(m$^2$ s) at 40°N, and ~181 gammas/(m$^2$ s) at 60°N. The neutron flux is ~12 neutrons/(m$^2$ s) at 0°N, ~15 neutrons/(m$^2$ s) at 20°N, ~24 neutrons/(m$^2$ s) at 40°N, and ~40 neutrons/(m$^2$ s) at 60°N. It is observed that both neutron and gamma fluxes are not changed at latitudes higher than 60° N. The various values of the neutron flux at sea level are reported in the literature: ~200 neutrons/(m$^2$ s) [40], ~125 neutrons/(m$^2$ s) [41], ~40 neutrons/(m$^2$ s) [42], ~31 neutrons/(m$^2$ s) [43], ~29 neutrons/(m$^2$ s) [44]. These variations in neutron numbers are due to a fact that measurements were performed at different latitudes using different experimental tools. More data on the neutron flux at various interfaces are summarized in Ref. [27].

### 3.1. Neutron and gamma lifetimes

The distributions of neutron and gamma lifetimes during a cascade air shower are shown in Figs. 2(a) and (b), respectively. The lifetime spectra are shown for three latitudes: 0°N, 40°N and 80°N. The area of particle collection is 100 m$^2$. The spectra are normalized by the total number of cosmic events (Monte Carlo histories) and shown in units 1/s. The lifetime distribution of neutrons (Fig. 2(a)) demonstrates a peak near ~50–70 μs. This is the most probable lifetime of neutrons during a cascade shower in each cosmic event. The number of neutrons with shorter and longer lifetimes is significantly decreased. Lifetimes of the longest-lived neutrons reach about 0.5–0.8 s. The spectrum of gamma lifetimes (Fig. 2(b)) shows a peak near ~50 μs. The peak of gammas is broader than that of neutrons. At peak, the number of gammas (Fig. 2(b)) is more than an order of magnitude higher compared to that of neutrons (Fig. 2(a)). The number of short-lived and long-lived gammas is again decreased on both side of the

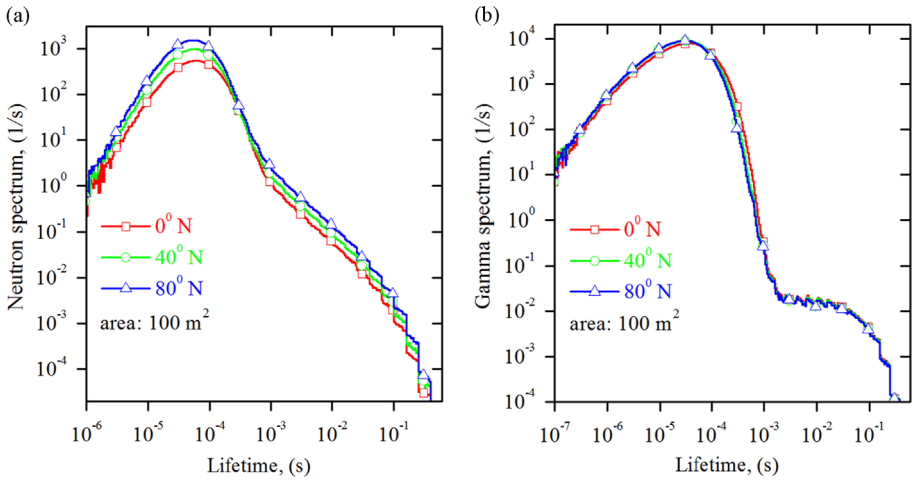


**Fig. 2.** Lifetime distribution of (a) neutrons and (b) gammas in a cosmic ray shower. The distributions of lifetime are illustrated for three latitudes (0°N, 40°N, and 80°N). Particle counts are collected within the area of 100 $m^2$ at sea level.

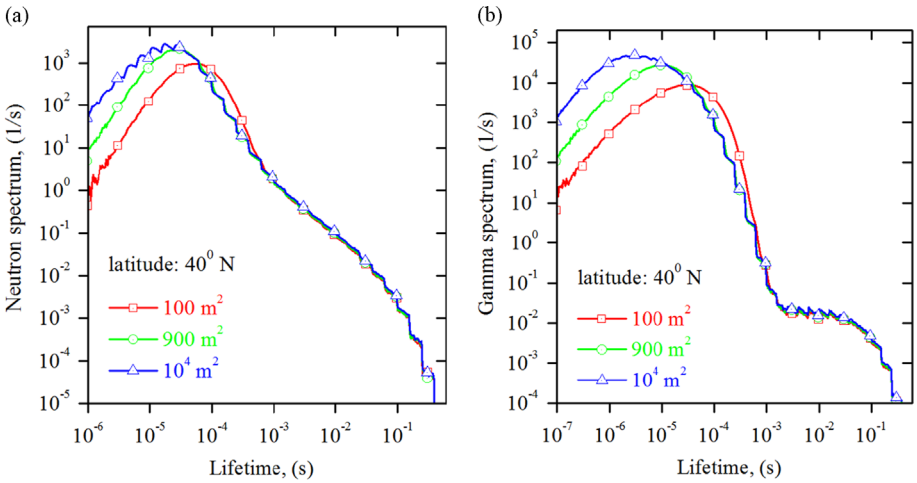


**Fig. 3.** The effect of the area size on lifetime distributions of (a) neutrons and (b) gammas in a cascade air shower. The lifetime distributions are shown for latitude of 40°N.

peak. However, the gamma spectrum shows a lifetime plateau within ~0.002–0.05 s. The nearly constant amount of gammas at these times could be due to the delayed radiative decay processes of excited air nuclei. Lifetimes of the longest-lived gammas in a cascade shower reach about 0.5 s. With the increase of latitude from 0°N to 60°N, the number of neutrons with the most probable lifetime increases, and the peak is slightly shifted toward shorter lifetimes (Fig. 2(a)). Above 60°N, it is observed that the spectrum is not changed with further increase of latitude. The effect of latitude on gamma lifetimes is insignificant (Fig. 2(b)). The effect of the area size on the distribution of neutron and gamma lifetimes in a cascade shower is shown in Fig. 3 for latitude of 40°N. Both neutrons and gammas with lifetimes less than ~1 ms are affected. Their number is increased with the increase of the area size, and the peak is shifted toward shorter lifetimes. The shift is slightly larger for gammas (Fig. 3(b)) compared to that of neutrons (Fig. 3(a)).

### 3.2. Multiplicity distributions of neutrons and gammas at sea level

The multiplicity (frequency) distribution of neutrons and gammas at latitude of 40°N is shown in Fig. 4. The distribution is normalized to the total number of sampled primary events. It is seen that the neutron multiplicity ranges from 0 to 12 neutrons depending on the size of the area (Fig. 4(a)). In most of the sampled events, we have observed zero neutrons at sea level. The probability for observation of one or two neutrons drops sharply about one to three orders of magnitude (Fig. 4(a)). However, there are very rare showers in which 5–12 neutrons can be generated. The gamma multiplicity ranges from 0 up to 120 gammas (Fig. 4(b)). The number of events with one gamma ray dominates. There is, however, a significant number of events in which zero gammas is also observed at sea level. The probability to observe two, three, or more gammas decreases sharply (Fig. 4(b)). The multiplicity of neutrons and gammas is affected by the size of the area. The secondary particles in extensive air showers can be spread over a large area causing very high multiplicity occurrences (up to 480 gammas is observed within the area of $10^4$ $m^2$ in one of rare events). The multiplicity curves of neutrons and gammas shown in Fig. 4 are slightly varied with the change of latitude (results are not shown).

### 3.3. Coincidence count distributions of neutron and gammas

The coincidence count distribution as opposed to multiplicity distribution is constructed in fixed time bins from the stream of neutrons and gammas originating from different showers. The simulated coincidence count distribution of neutrons within the area of 100 $m^2$ at latitude of 40°N and fixed time intervals of 50 μs, 500 μs, 1000 μs, and 2000 μs and their comparison to a Poisson

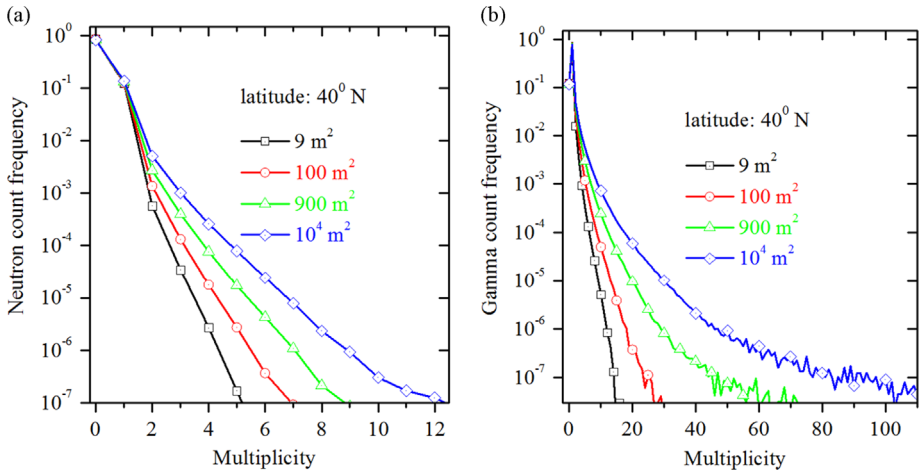


**Fig. 4.** Multiplicity distributions of cosmic-ray-induced (a) neutrons and (b) gammas at latitude 40°N. Multiplicities are calculated within the area of 9 $m^2$, 100 $m^2$, 900 $m^2$ and $10^4$ $m^2$ at sea level.

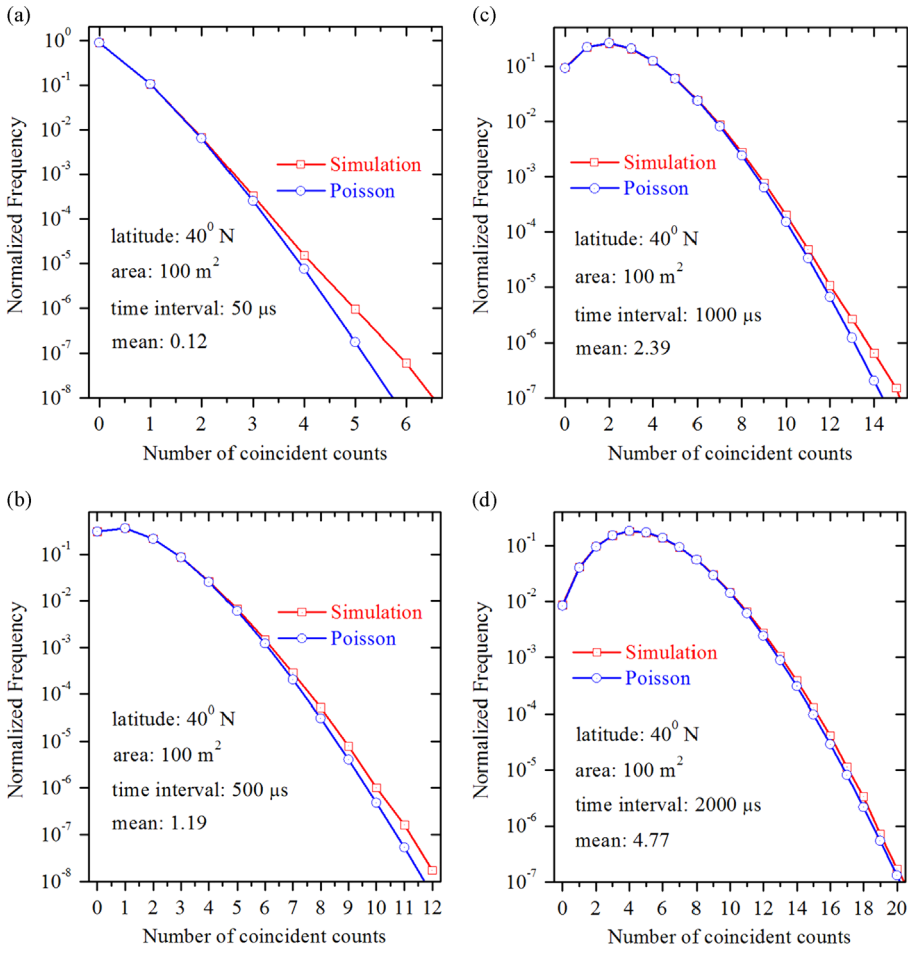


**Fig. 5.** Simulated coincidence count distributions of neutrons (red curves) at sea level for time intervals of (a) 50 μs, (b) 500 μs, (c) 1000 μs, and (d) 2000 μs, compared to a theoretical Poisson distribution (blue curves) with the same mean. The area for particle count collection is 100 $m^2$. The latitude is 40°N. (For interpretation of the references to color in this figure legend, the reader is referred to the web version of this article.)

distribution with the same count rate is shown in Fig. 5. The same distributions of neutrons calculated within the area of 900 $m^2$ at latitude of 40°N are illustrated in Fig. 6. These plots give an idea how the coincidence counting is changing as a function of the width of time intervals (bins) and the size of the area within which neutron counts are collected. Within the area of 100 $m^2$, most of time intervals with the width of 50 μs are empty (Fig. 5(a)), i.e., they contain zero coincidence counts. The probability to observe 1, 2, 3, etc. coincidence counts of neutrons drops down very sharply. The mean (average) number of neutron coincidence counts is 0.12. The shape of the curve is nearly a straight line. With the increase of the width of time interval by an order of magnitude (to 500 μs), the line-shaped curve is transformed to truncated hill-shaped curve with the mean of 1.19 (Fig. 5(b)). Almost one hundred

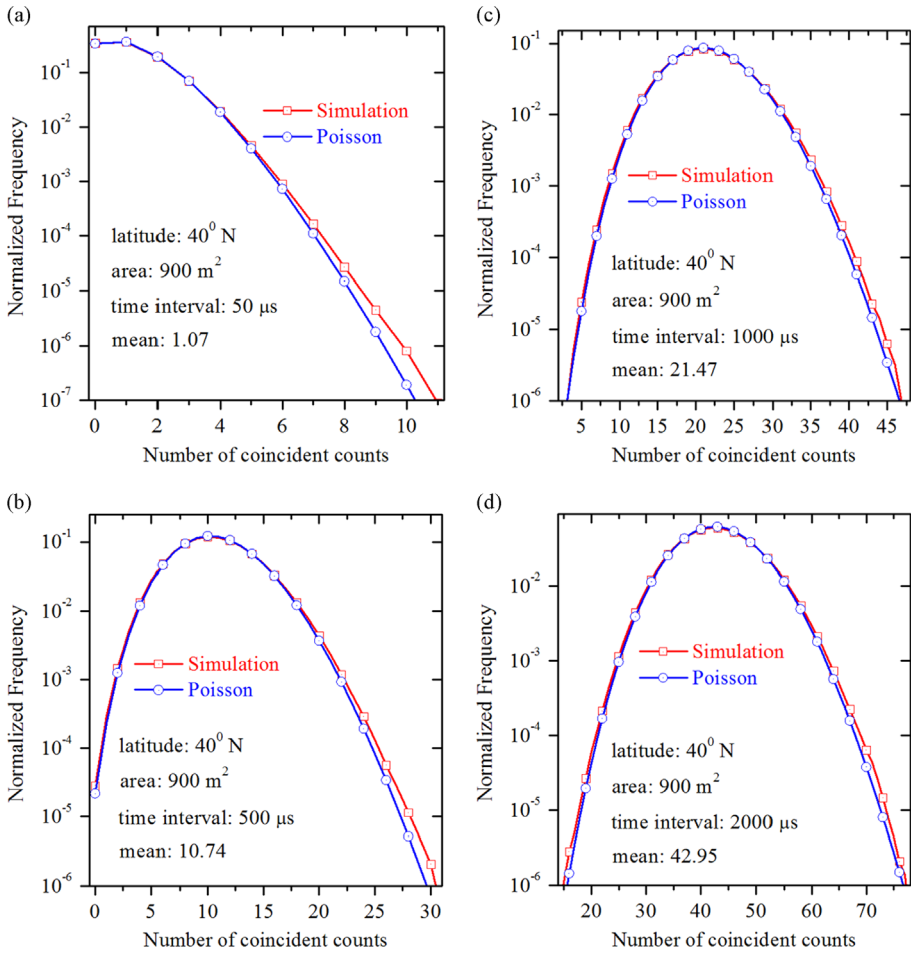


**Fig. 6.** Simulated coincidence count distributions of neutrons (red curves) at sea level for time intervals of (a) 50 μs, (b) 500 μs, (c) 1000 μs, and (d) 2000 μs, compared to a theoretical Poisson distribution (blue curves) with the same mean. The area for particle count collection is 900 $m^2$. The latitude is 40°N. (For interpretation of the references to color in this figure legend, the reader is referred to the web version of this article.)

percent of the distribution lies yet to the right of the mean. With further increase of the width of time interval to 1000 μs (Fig. 5(c)) and 2000 μs (Fig. 5(d)), the mean value is increased to 2.39 and 4.77 neutron coincidence counts, respectively. The curve starts to fall off on the left side of the mean. It is seen that a portion of the distribution belonging to the left of the mean increases (Fig. 5(d)). However, even at large widths of time interval (~2000 μs), the coincidence count distribution of neutrons within the area of 100 $m^2$ is still asymmetric. The size of the area has a major impact on the shape of coincidence curves. It is observed that the curves remain nearly line-shaped even for the time interval of 2000 μs, when the size of the area is 1 $m^2$ or 9 $m^2$. The mean is 0.43 within the area of 9 $m^2$ in fixed interval of 2000 μs (results not shown). In the case of the area of 900 $m^2$, the coincidence distribution with the mean of 1.07 is already hill-shaped in time interval of 50 μs (Fig. 6(a)). For larger widths of time intervals, the neutron counts are distributed equally on both sides of the mean (Fig. 6(c) and (d)). For the area of $10^4$ $m^2$, the coincidence count distribution in time interval of 10 μs with the mean of 17.5 is equally hill-shaped on either side of the mean (results not shown). It is seen in Figs. 5 and 6 that the simulated coincidence distributions of neutrons (red curves) deviate from a Poisson distribution (blue curves) with the same mean. The increased variance of the simulated distribution compared to a Poisson distribution is indicative of the time-correlated processes.

The coincidence count distributions of gammas derived for the area of 100 $m^2$ and 900 $m^2$ at latitude of 40°N are shown in Figs. 7 and 8, respectively. The simulated coincidence curves are plotted for time intervals of 50 μs, 500 μs, 1000 μs, and 2000 μs and compared to a theoretical Poisson distribution with the same mean. The number of gamma counts at the sea level is significantly higher compared to that of neutrons. Therefore, the counting statistic of gammas is strongly enhanced. As in the case of neutrons (Figs. 5 and 6), the shape of the curves (Figs. 7 and 8) changes depending on the mean. The distribution of gamma counts transforms from a truncated asymmetric hill-shaped profile (Fig. 7(a)) to a nearly symmetric hill-shaped profile (Fig. 7(d)). With the increase of the area from 100 $m^2$ to 900 $m^2$, the number of coincidence counts in time intervals increases considerably (Fig. 8). The simulated count distribution of gammas (red curves) shows a dramatic increase in variance compared to a Poisson distribution (blue curves). The variance is significantly wider than that expected if the source of gammas was purely random (Poisson curve).

### 3.4. Feynman-Y excess variance

The Feynman-Y excess variance [35] in the coincidence count distribution is shown in Fig. 9(a) and (b) for neutrons and gammas, respectively. This excess variance is indicative of time-correlated multiplying processes in cascades of air showers. If the neutrons and gammas have arrived randomly at the sea level, the Feynman-Y could be zero. The Feynman-Y curves are plotted for the various sizes of the irradiated area at latitude of 40°. It is evident for both neutrons and gammas that the excess variance is greater for larger sizes of the area. The Feynman-Y of neutrons is about an order of

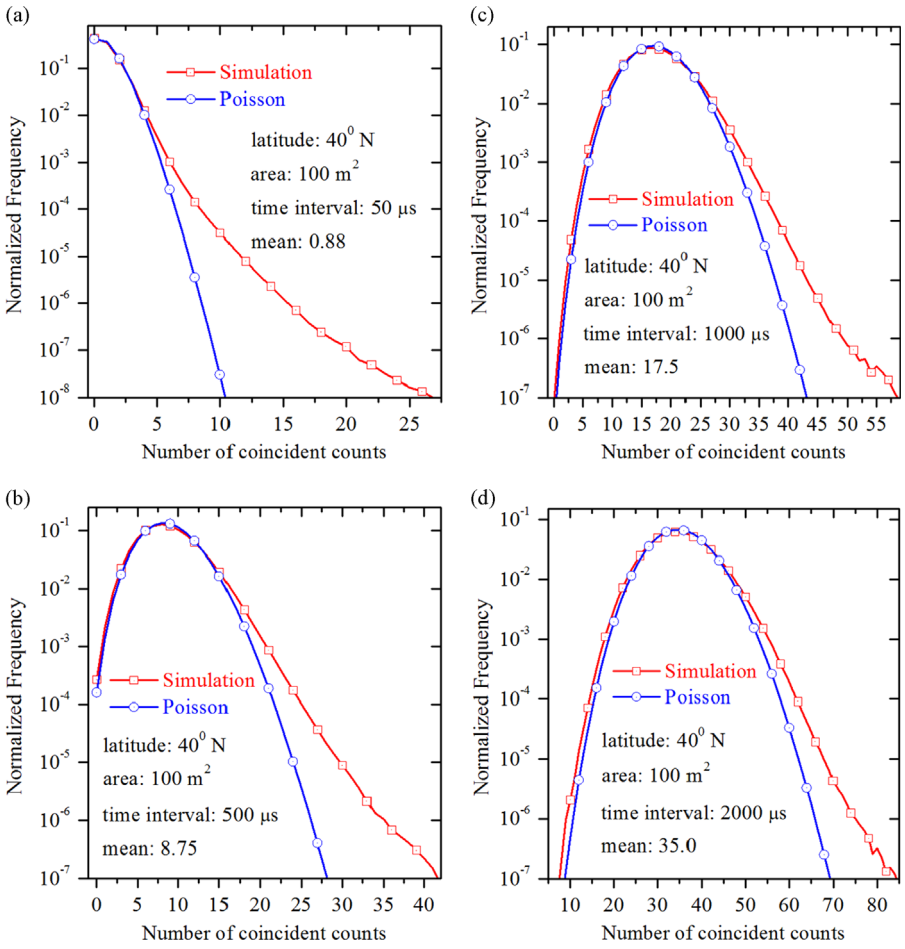


**Fig. 7.** Simulated coincidence count distributions of gammas (red curves) at sea level for fixed time intervals of (a) 50 μs, (b) 500 μs, (c) 1000 μs, and (d) 2000 μs. The blue curves are theoretical Poisson distributions with the same mean. The count of particles is collected within the specified area of 100 $m^2$ at latitude of 40°N. (For interpretation of the references to color in this figure legend, the reader is referred to the web version of this article.)

magnitude lower than that of gammas. The Feynman-Y curves rise from zero during ~250 μs and then reach an asymptotic *Y* value dependent on the area size.

## 4. Discussion

We have developed a computational model to explore time correlations of cosmic-ray-induced background of neutrons and gammas at sea level. The arrival-time distributions of neutrons and gammas are generated from the CRY library [34] and then used as input data in our MONSOL code to calculate their lifetimes, multiplicities, coincidence count statistic, and Feynman-Y excess variance. The cosmic-ray-induced neutron and gamma flux at sea level results from interactions starting in the upper atmosphere. The probability of particle surviving from the point of birth to sea level depends on the specific interaction mechanisms. Many neutrons and gammas are produced locally in sub-cascades at different depths in the atmosphere. We find that the majority of neutrons and gammas arrive within the time window of 10–100 μs (Fig. 2). The times of arrival of neutrons have been previously reported from the MCNPX calculations [26]. However, those results show that the peak of neutron lifetime drops abruptly at ~200 μs. The neutrons with shorter lifetimes $< \sim 200$ μs are not presented [26]. In agreement with our results (Figs. 2(a) and 3(a)), the number of neutrons with longer lifetimes decreases by seven orders of magnitude from a maximum value at ~200 μs to much lower value at ~0.5 s. The number of neutrons and gammas arrived at sea level in each sampled cosmic event are counted within a specified area and multiplicity distributions are built. We find that the occurrence of zero neutrons and one gamma ray at sea level are the most frequent observations (Fig. 4). There are, however, the rare air showers in which up to ~12 neutrons and ~120 gammas can be generated within the area of $10^4$ $m^2$.

The coincidence count statistic can be used to distinguish the time-correlated neutrons produced in the spallation events from neutrons distributed randomly in time such as those originating from a radioactive decay of heavy nuclei. The Poisson distribution can be used to describe independent and random events that occur at a fixed mean rate. So, we can use the Poisson statistics to model the count distribution of uncorrelated neutrons. However, the spallation of air nuclei by cosmic rays is a fission-like process that is similar to the induced nuclear fission. An energetic projectile undergoes a number of collisions with nucleons in the nucleus ejecting a cascade of neutrons and protons. The remaining excitation of the target nucleus is released through the "evaporation" process with the emission of nuclear particles and gammas. The neutrons and gammas originating from spallation and evaporation of air nuclei are not randomly distributed in time, but rather they occur as time-correlated groups. The wider variance of the number of neutron and gamma counts in fixed time intervals compared to a Poisson distribution (Figs. 5–8) is a clear evidence of multiplying processes in air showers. It should be noted that the simulated and Poisson distributions of neutrons are very close (Figs. 5 and 6). This means that spallation and evaporation of neutrons are low-multiplying processes. The count distribution

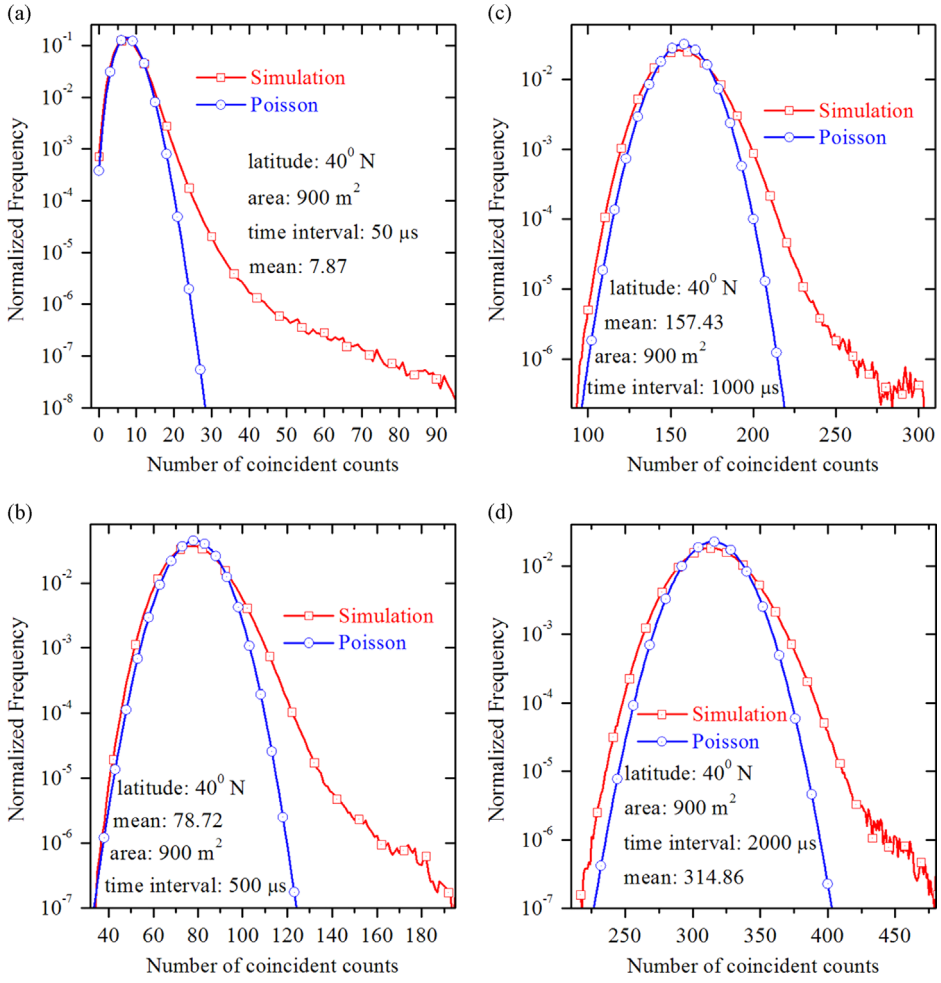


**Fig. 8.** Simulated coincidence count distributions of gammas (red curves) at sea level for fixed time intervals of (a) 50 μs, (b) 500 μs, (c) 1000 μs, and (d) 2000 μs. The blue curves are theoretical Poisson distributions with the same mean. The count of particles is collected within the specified area of 900 $m^2$ at latitude of 40°N. (For interpretation of the references to color in this figure legend, the reader is referred to the web version of this article.)

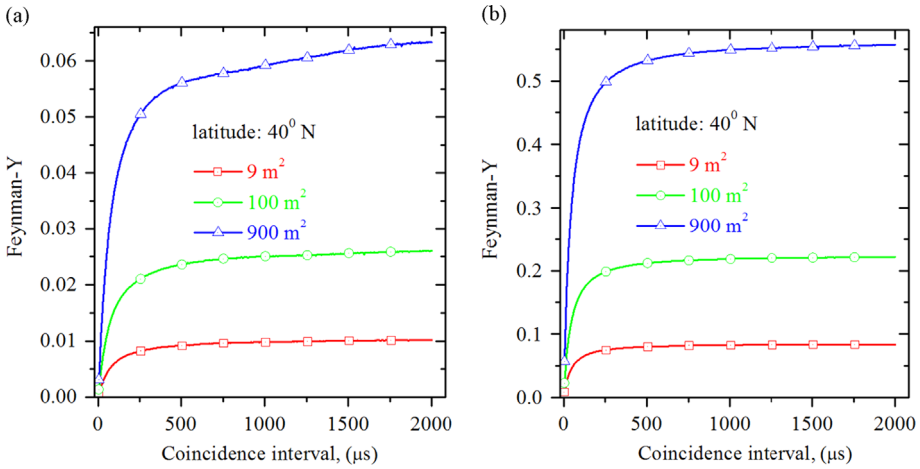


**Fig. 9.** The calculated Feynman-Y excess variance as a function of time interval for (a) neutrons and (b) gammas. The Feynman-Y curves are shown for three sizes of the area (9 $m^2$, 100 $m^2$, and 900 $m^2$) where particle counts are collected. The latitude is 40°N.

with a larger tail of high-order coincidences should be expected for high-multiplying sources. The simulated part of the distribution corresponding to low-order coincidences is the same as a Poisson distribution. For high-order coincidences, the count distribution tail is clearly seen to deviate from the Poisson part of the distribution. For short time intervals (~50 μs), the deviation is larger (Figs. 5(a) and 6(a)). The cosmic-ray-induced neutron background calculated in a 2000 μs interval is nearly a Poisson distribution (Figs. 5(d) and 6(d)). These results suggest that the simulated coincidence count distribution of cosmic-ray-induced neutrons is a Poisson distribution on a long time scale, but it has the non-Poisson tail on short time scales. This behavior was reported in the previous study [27]. The simulated coincidence count distributions of gammas noticeably diverge from a Poisson

distribution with the excess of high-number coincidences (Figs. 7 and 8). For both short and long time intervals, the calculated distribution is much wider than the corresponding Poisson distribution with the same mean. This larger deviation from Poisson indicates higher multiplication rate of gammas in the air shower compared to that of neutrons.

The presence of time-correlated neutrons and gammas is well determined by the amount by which the variance-to-mean (known as the Feynman variance) exceeds unity. For an uncorrelated Poisson source, the Feynman variance is zero. An excess of variance (Fig. 9) indicates time-correlated multiplying processes in air showers. During $\sim$250 μs, the *Y*-variance rises from zero (very short coincidence intervals) to an asymptote (long coincidence intervals). For short time intervals ($<5$ μs), the coincidence counts are approximately Poisson distributed, i.e. $Y\sim 0$. There are no time correlations occurring on these short time scales. For time intervals with larger widths ($\sim$10–100 μs), the *Y*-distribution is built from counts originating from portions of multiplication chains. For very long time intervals ($>250$ μs), the coincidence counts are collected from a whole multiplying chain or many such chains. In this case, the width of time interval is larger than the duration of time-correlated multiplying processes in air showers. The Feynman-Y variance increases with the area size, since the number of counts is greater within the larger area. The value of *Y* is about an order of magnitude smaller for neutrons compared to that of gammas (Fig. 9).

## 5. Conclusions

The time-correlated neutrons and gammas originate primarily from spallation and evaporation reactions of air nuclei. The gamma rays are also generated in the electromagnetic cascade showers. The time-correlated radiation background produced by cosmic events can interfere with neutrons and gammas emitted by fission sources, thus making their detection and identification very difficult. Therefore, the understanding of statistical aspects of the time correlation of cosmic-ray-induced neutrons and gammas at sea level is of great practical importance. We developed a computational model (MONSOL code) based on the CRY library to study time-correlations of cosmic-ray-induced background of neutrons and gamma rays at sea level. The lifetime and multiplicity distributions, coincidence count statistic, and excess variance of neutrons and gammas in air showers are analyzed. It is found that the effective lifetime of neutrons and gammas in air showers is within a range of $\sim$10–100 μs. In an extensive air shower, the neutron lifetime can reach $\sim$0.5 s, agreeing with previous results from MCNPX simulations. Based on the multiplicity distribution, most of the time it is observed zero neutrons and one gamma ray at sea level. The tail of multiplicity distribution of gamma rays is considerably wider compared to that of neutrons implying the higher rate of gamma-multiplying processes. The cosmic-ray-induced background of neutrons and gammas at sea level is found to be time-correlated, since their coincidence count distribution deviates from a Poisson distribution. The Feynman-Y variance-to-mean is greater for gammas than that for neutrons. Depending on the area size, the excess variance is about $\sim$1–6% for neutrons and $\sim$10–60% for gammas. Also, we find that the longest duration of time-correlated neutron and gamma-multiplication processes in air showers is less than $\sim$250 μs.

## Acknowledgments

This work is sponsored by the U.S. Department of Energy (DOE), the National Nuclear Security Administration (NNSA), Office of Proliferation Detection (NA-221) under Grant No. DE-NA0000533.

## References

[1] R. Silberberg, C.H. Tsao, Phys. Rep. 191 (1990) 351.
[2] T. Stanev, High Energy Cosmic Rays, second ed., Springer, Praxis, Berlin; New York, Chichester, UK, 2009.
[3] P.K.F. Grieder, Cosmic Rays at Earth: Researcher's Reference Manual and Data Book, first ed., Elsevier Science Ltd., Amsterdam; New York, 2001.
[4] M. Nieminen, J.J. Torsti, E. Valtonen, H. Arvela, M. Lumme, J. Peltonen, E. Vainikka, J. Phys. G 11 (1985) 421.
[5] J.W. Norbury, J. Phys. G 32 (2006) B31.
[6] K. Mitsui, Y. Minorikawa, H. Komori, Phys. Rev. D 44 (1991) 661.
[7] C. Aguirre, H. Aoki, K. Hashimoto, K. Honda, N. Inoue, N. Kawasumi, Y. Maeda, N. Martinic, T. Matano, N. Ohmori, A. Ohsawa, K. Shinozaki, M. Tamada, R. Ticona, I. Tsushima, Phys. Rev. D 62 (2000) 032003.
[8] H.J. Drescher, G.R. Farrar, Phys. Rev. D 67 (2003) 116001.
[9] S.M.H. Halataei, M. Bahmanabadi, M.K. Ghomi, J. Samimi, Phys. Rev. D 77 (2008) 083001.
[10] C.A.G. Canal, S.J. Sciutto, T. Tarutina, Phys. Rev. D 79 (2009) 054006.
[11] R. Ulrich, Phys. Rev. D 83 (2011) 054026.
[12] J. Liu, Q. Yuan, X.J. Bi, H. Li, X.M. Zhang, Phys. Rev. D 85 (2012) 043507.
[13] P. Bassi, G. Clark, B. Rossi, Phys. Rev. 92 (1953) 441.
[14] J. Linsley, L. Scarsi, Phys. Rev. 128 (1962) 2384.
[15] M.A. Locci, P. Picchi, G. Verri, Nuovo Cimento B 50 (1967) 384.
[16] C.P. Woidneck, E. Bohm, J. Phys. A 8 (1975) 997.
[17] N. Inoue, Y. Toyoda, T. Maeda, M. Kawamoto, M. Shigeta, K. Kihara, J. Phys. G 15 (1989) 1899.
[18] P.R. Blake, D.M. Mann, W.F. Nash, B. Oconnell, R.B. Strutt, J. Phys. G 8 (1982) 1605.
[19] F. Kakimoto, T. Kaneko, Y. Mizumoto, K. Suga, N. Inoue, K. Nishi, Y. Yamada, N. Tajima, E. Gotoh, H. Nakatani, H. Yoshii, R. Anda, C. Aguirre, P.K. Mackeown, K. Murakami, T. Hara, Y. Toyoda, T. Maeda, J. Phys. G 9 (1983) 339.
[20] E.J. Devilliers, D.J. Vanderwalt, P.K.F. Grieder, G. Vanurk, J. Phys. G 12 (1986) 547.
[21] A.J. Baxter, J. Phys. A 2 (1969) 50.
[22] G. Battistoni, A. Ferrari, M. Carboni, V. Patera, Astropart. Phys. 9 (1998) 277.
[23] Y.A. Fomin, G.V. Kulikov, M.Y. Zotov, Astropart. Phys. 20 (2004) 413.
[24] N. Ochi, A. Iyono, H. Kimura, T. Konishi, T. Nakamura, T. Nakatsuka, S. Ohara, N. Ohmori, K. Okei, K. Saitoh, N. Takahashi, S. Tsuji, T. Wada, I. Yamamoto, Y. Yamashita, Y. Yanagimoto, J. Phys. G 29 (2003) 1169.
[25] S. Croft, L.C.A. Bourva, Nucl. Instrum. Methods Phys. Res., Sect. A 505 (2003) 536.
[26] C.R. Heimbach, J. Res. Natl. Inst. Stand. Technol. 112 (2007) 95.
[27] R.T. Kouzes, J.H. Ely, A. Seifert, E.R. Siciliano, D.R. Weller, L.K. Windsor, M.L. Woodring, J. Borgardt, E. Buckley, E. Flumerfelt, A. Oliveri, M. Salvitti, Nucl. Instrum. Methods Phys. Res., Sect. A 587 (2008) 89.
[28] K.J. Orford, J. Phys. G 26 (2000) R1.
[29] T. Gozani, IEEE Trans. Nucl. Sci. NS 56 (2009) 736.
[30] D.R. Beaulieu, D. Gorelikov, H. Klotzsch, P. de Rouffignac, K. Saadatmand, K. Stenton, N. Sullivan, A.S. Tremsin, IEEE Technol. Homeland Secur. HST '09 (2009) 295.
[31] R.C. Runkle, D.L. Chichester, S.J. Thompson, Nucl. Instrum. Methods Phys. Res., Sect. A 663 (2012) 75.
[32] P.A. Hausladen, J.T. Mihalczo, B.W. Blackburn, S.M. Watson, J.L. Jones, A.W. Hunt, S. Thompson, Identifying nuclear material via prompt photo-neutron multiplicity measurements, in: Proceedings of the CP1099 20th International Conference on Applications of Accelerators in Research and Industry, American Institute of Physics, 2009, pp. 670–675.
[33] F. Ferrari, P. Peerani, Radiat. Meas. 45 (2010) 1034.
[34] C. Hagmann, D. Lange, D. Wright, Cosmic-ray shower generator (CRY) for Monte Carlo transport codes, in: Proceedings of the IEEE Nuclear Science Symposium Conference Record, NSS '07, 2007, pp. 1143–1146.
[35] S. Croft, A. Favalli, D.K. Hauck, D. Henzlova, P.A. Santi, Nucl. Instrum. Methods Phys. Res., Sect. A 686 (2012) 136.
[36] P. Papini, C. Grimani, S.A. Stephens, Nuovo Cimento C 19 (1996) 367.
[37] K. Ide, M.F. Becchetti, M. Flaska, A. Poitrasson-Riviere, M.C. Hamel, J.K. Polack, C.C. Lawrence, S.D. Clarke, S.A. Pozzi, Nucl. Instrum. Methods Phys. Res., Sect. A 694 (2012) 24.
[38] E. Aguayo, R.T. Kouzes, J.L. Orrell, Monte carlo simulations of cosmic ray hadronic interactions, Pacific Northwest National Laboratory Report No. PNNL-20401, 2010.
[39] E. Aguayo, R.T. Kouzes, A.S. Ankney, J.L. Orrell, T.J. Berguson, M.D. Troy, Cosmic ray interactions in shielding materials, Pacific Northwest National Laboratory Report No. PNNL-20693, 2011.
[40] R.M. Lindstrom, D.J. Lindstrom, L.A. Slaback, J.K. Langland, Nucl. Instrum. Methods Phys. Res., Sect. A 299 (1990) 425.
[41] B. Wiegel, A.V. Alevra, M. Matzke, U.J. Schrewe, J. Wittstock, Nucl. Instrum. Methods Phys. Res., Sect. A 476 (2002) 52.
[42] M. Yamashita, L.D. Stephens, H.W. Patterso, J. Geophys. Res. 71 (1966) 3817.
[43] K. O'Brien, H.A. Sandmeier, G.E. Hansen, J.E. Campbell, J. Geophys. Res. 83 (1978) 114.
[44] R.J. Sheu, J.S. Lin, S.H. Jiang, Nucl. Instrum. Methods Phys. Res., Sect. A 476 (2002) 74.